
Article:
Yang, W., Li, Y., Liu, W. orcid.org/0000-0003-2968-2888 et al. (3 more authors) (2021) Scalloping suppression for ScanSAR images based on modified Kalman filter with preprocessing. IEEE Transactions on Geoscience and Remote Sensing, 59 (9). pp. 7535-7546. ISSN 0196-2892

https://doi.org/10.1109/tgrs.2020.3034098

Scalloping Suppression for ScanSAR Images Based on Modified Kalman Filter With Pre-processing

Wei Yang, *Member*, *IEEE*, Yihan Li, Wei Liu, *Senior Member*, *IEEE*, Jie Chen, *Senior Member*, *IEEE*, Chunsheng Li, and Zhirong Men, *Member*, *IEEE*

***Abstract*—Scanning Synthetic Aperture Radar (ScanSAR) mode is widely used in Earth observation because of its capability of acquiring wide-swath images with moderate resolution. However, due to the operation mechanism of ScanSAR mode, the acquired images often suffer from the scalloping problem, resulting in significant deterioration of image quality. In this paper, a novel scalloping suppression method is proposed for ScanSAR images, based on modified Kalman filter with pre-processing. Firstly, an image model is built to analyze the effect caused by scalloping. Then, a modified Kalman filter is proposed to estimate the intensity of scalloping. However, if the scene is complicated or the scalloping effect is strong, Kalman filter works with poor performance. Therefore, an innovative pre-processing operation is introduced, involving image segmentation and pixel value filling. Finally, the proposed method is verified by GaoFen-3 (GF-3) and TerraSAR-X satellite images with different scenes. The results demonstrate that the proposed method can accommodate the complex scene well and achieve effective scalloping suppression.**

***Index Terms*—ScanSAR, scalloping suppression, modified Kalman filter, GaoFen-3 satellite.**

I. Introduction

SCANNING Synthetic Aperture Radar (ScanSAR) mode is easy to operate and has a wide-swath coverage, and therefore it has been widely used in both military and civilian fields [1]. The ScanSAR mode realizes wide swath by periodically switching the antenna elevation beam to different range sub-swaths. As for each of the imaged sub-swaths, targets located in different azimuth positions will have different amplitude weighting due to the azimuth antenna pattern (AAP), resulting in a periodic azimuth-varying amplitude modulation, namely the scalloping effect, and periodic light-dark stripes in the image, as shown in Fig. 1. Therefore, scalloping suppression has become an important problem to be treated in SAR image processing [2-4].

The most common scalloping suppression technique is to correct this periodic variation directly on the raw echo data, by evaluating and compensating the inverse antenna pattern during the image focusing [5-8]. However, this method can only be applied to high SNR scenarios and the performance will be significantly affected by the antenna beam pointing error. In addition, the terrain observation with progressive scan (TOPS) mode is developed, by steering the azimuth antenna beam throughout the acquisition from backward to forward in azimuth, which eliminates scalloping [2]. But, to realize TOPS mode, the sensor will be more complex, as well as the imager focusing operation.

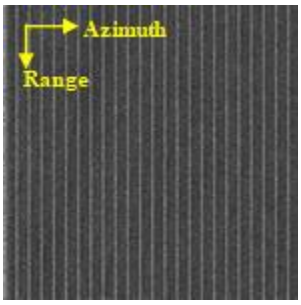

Fig. 1. SAR image affected by the scalloping effect.

In recent years, several image-based methods have been discussed and proposed. In [9], a scalloping suppression filter is proposed, which calibrates scalloping in the image spectrum by identifying the scalloping related peaks. And, a wavelet transform based method is also introduced, suppressing scalloping by wavelet multi-resolution analysis [10]. These two methods work well for ScanSAR images, but suffer from very high computational complexity and loss of radiometric accuracy. To resolve this problem, a method for scalloping intensity estimation using Kalman filter is proposed, which can suppress the scalloping effect effectively while maintaining image radiometric accuracy [11]. Furthermore, this method exhibits great potential as a post-processing tool for ScanSAR images in practice. However, due to the linearity and Gaussianity requirement of Kalman filter, the applicability of this method is limited, since the amplitude of SAR image normally follows the Rayleigh distribution. An attempt has been made in [12] to solve this problem, in which image segmentation and pixel value filling are introduced to modify

This Manuscript received January 19, 2020. This work was supported by the National Natural Science Foundation of China under Grant 61701012.

W. Yang is with the School of Electronic and Information Engineering, Beihang University, Beijing 100191, China (e-mail: yangweigigi@sina.com).

Y. Li is with the School of Electronic and Information Engineering, Beihang University, Beijing 100191, China (e-mail: 727324342@qq.com).

W. Liu is with the Department of Electronic and Electrical Engineering, University of Sheffield, Sheffield, S13JD, U.K. (e-mail: w.liu@sheffield.ac.uk).

J. Chen is with the School of Electronic and Information Engineering, Beihang University, Beijing 100191, China (e-mail: chenjie@buaa.edu.cn).

C. Li is with the School of Electronic and Information Engineering, Beihang University, Beijing 100191, China (e-mail: lics@buaa.edu.cn).

Z. Men is with the School of Electronic and Information Engineering, Beihang University, Beijing 100191, China (e-mail: menzhirong@buaa.edu.cn).

the distribution of amplitude and improve the performance. But the segmentation threshold selection and the pixel completion scheme are empirical, limiting its practicality and leading to failures in some complicated scenes.

In this paper, a novel scalloping suppression method is proposed based on modified Kalman filter with pre-processing. To improve the robustness of the method, the condition for applying Kalman filter on ScanSAR image is analyzed, which shows that the suppression performance of Kalman filter is affected by the statistical distribution of image. Therefore, the Jarque-Bera test is adopted to measure the applicability of Kalman filter quantitatively. Then, a novel pre-processing operation is presented based on the Jarque-Bera value, which ensures the following Kalman filtering operation to accommodate different scenes of SAR image. In this pre-processing operation, the image is divided into two sub-images by selecting an appropriate threshold, which is calculated by a genetic algorithm and chosen based on the maximum between-cluster variance principle. As for each sub-image, missing pixels will be filled to satisfy the Gaussian distribution requirement of Kalman filter. Consequently, Kalman filtering is performed on each sub-image for scalloping estimation and suppression, respectively. Then, sub-images fusion is implemented by only preserving the pixels from the original input image. Finally, the proposed method is verified by GF-3 and TerraSAR-X images, with corresponding analysis and discussion. The results demonstrate that the proposed method can accommodate the complex scene well and achieve effective scalloping suppression.

This paper is organized as follows. An overview of the ScanSAR mode and the modified Kalman filer for scalloping removal are presented in Section II. Analysis of the Kalman filter's limitation is analyzed in Section III, followed by the proposed method in Section IV. Experimental results for scalloping suppression on GF-3 and TerraSAR images are provided in Section V and conclusions are drawn in Section VI.

II. Scalloping Removal With Modified Kalman Filter

In this section, a simplified geometry of the ScanSAR mode together with working mechanism is reviewed, firstly. By analyzing the properties of ScanSAR image, an image model is then introduced for describing the scalloping effect. Finally, a modified Kalman filter is provided for scalloping estimation.

A. ScanSAR Model

In ScanSAR mode, azimuth resolution is traded off for swath coverage. To obtain a wide-swath in range, the antenna elevation beam of ScanSAR mode is steered to different contiguous range sub-swaths periodically, as shown in Fig. 2. As a result, for each sub-swath, the dwell time is reduced compared to the stripmap mode, and the scene is illuminated by the antenna beam for a short time interval, which is dependent on the azimuth resolution and the number of sub-swaths [12]. Note that each target is illuminated with only a small portion of the azimuth antenna pattern (AAP), and targets located in different azimuth positions will be weighted by different portions of the AAP, resulting in non-stationarity of amplitudes in azimuth. Consequently, the scalloping effect appears after image formation processing, as illustrated in Fig. 3.

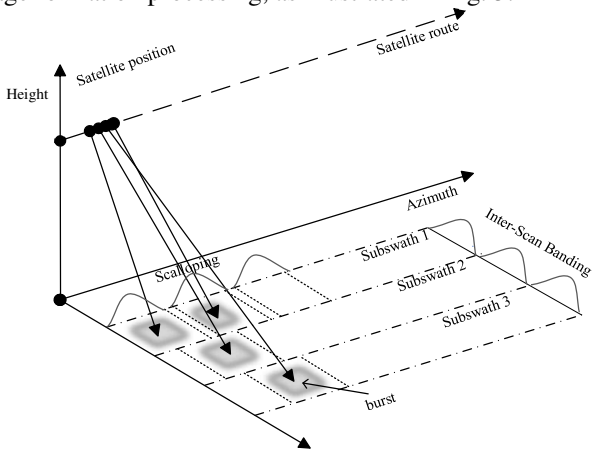

Fig. 2. ScanSAR acquisition geometry.

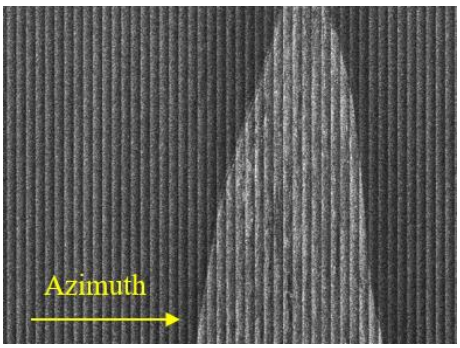

Fig. 3. Scalloping in a GF-3 ScanSAR image for one sub-swath.

B. Removal of Scalloping

Although the scalloping effect can be suppressed partly by antenna pattern correction during the image focusing, the residual scalloping effect still affects image quality significantly, due to antenna beam pointing error, antenna beam pattern error, and noise. Therefore, to describe the scalloping effect, a ScanSAR image model suffering from scalloping is given by [11,12]

$$O_S(r,a) = I_S(r,a) \quad - \quad I_O(r,a) \quad r \in [1,R] \quad a \in [1,A] \quad (1)$$

where $I_O(r,a)$ indicates the ideal two-dimensional amplitude image without scalloping interference, $I_s(r,a)$ indicates the interfered image with scalloping, and $O_s(r,a)$ indicates the scalloping on image. *R* and *A* are the number of range sampling points and the number of azimuth frame, respectively. *r* and *a* correspond to the position of a pixel in range and azimuth. Then, $I_O(r,a)$, $I_s(r,a)$, and $O_s(r,a)$ can be regarded as two-dimensional matrices.

Since the range antenna pattern correction is usually performed during the image focusing, the scalloping variation in range is very small. For sake of simplicity without losing generality, the intensity of scalloping is treated as a constant value along the range direction in this paper. Note that if range variation of scalloping effect is obvious, image division along range direction can be implemented to accommodate this problem.

Consequently, for an arbitrary frame in azimuth, equation (1) can be rewritten as

$$I_S(r) = I_O(r) + O_S \qquad r \in [1, R] \tag{2}$$

where O_S is a constant component attached to $I_O(r)$.

Considering $I_O(r)$ is a noise signal term, the problem of scalloping estimation is then transformed into the estimation of a direct current component in the presence of noise. Consequently, an innovative idea is proposed for scalloping estimation using the Kalman filtering process, in which I_S is the output of a linear system and O_S is the state value to be estimated.

As for a discrete-time process, to estimate the state value, the following stochastic difference equation is usually used [14]

$$x_k = Ax_{k-1} + \omega_{k-1} \tag{3}$$

where x represents the state of O_S, A is the state transition matrix, ω is the process noise.

Then, define the observation equation as

$$z_k = H\ x_k + v_k \tag{4}$$

where z represents the observed state of O_S, H is the observation gain matrix, v is the observation noise.

Usually, they are assumed to be independent white Gaussian, i.e.,

$$p(\omega) \sim N(0, Q) \tag{5}$$

$$p(v) \sim N(0, \Re) \tag{6}$$

where $p(\bullet)$ is the probability density function, Q represents the variance of system noise and $\Re$ is the variance of observation noise.

In view of (2), O_S is the item to be estimated. Since O_S is a constant, its state does not change, and therefore, parameter A in (3) is 1. $I_0(r), r \in [1, R]$ is the observation noise in (4). In this estimation, the pixel value of the interfered image is the measurement value of the system, and there is no other gain, and consequently, the value of H in (4) is 1. Based on the above model, a prior estimate covariance and posterior estimate covariance of the system can be written as

$$P_k^- = E\left[(x_k - \hat{x}_k^-)(x_k - \hat{x}_k^-)^T\right] \tag{7}$$

$$P_k = E\left[(x_k - \hat{x}_k)(x_k - \hat{x}_k)^T\right] \tag{8}$$

where $\hat{x}_k^-$ and $\hat{x}_k$ are the k_{th} prior estimate and posterior estimate of system state, respectively. Then, the time update equations and the state update equations of the Kalman filter are obtained as follows.

Prediction equation:

$$\hat{x}_k^- = \hat{x}_{k-1} \tag{9}$$

$$P_k^- = P_{k-1} + Q \tag{10}$$

Update equation:

$$K_k = \frac{P_k^-}{P_k^- + \Re} \tag{11}$$

$$\hat{x}_k = \hat{x}_k^- + K_k\left(z_k - \hat{x}_k^-\right) \tag{12}$$

$$P_k = (I - K_k)P_k^- \tag{13}$$

where K_k is the blending factor that minimizes a posteriori error covariance; Q and $\Re$ are the covariances of process noise and observation noise, respectively; I is a unity matrix.

In each column, the Kalman filter with multiple iterations can accurately estimate the intensity of scalloping, which can be subtracted from each column for scalloping suppression.

III. Conditions for Kalman filter's applicability

However, the estimation method mentioned above sometimes does not achieve the desired effect in practice, especially for complex scene. Detailed analysis and experiments indicate that this is related to the statistical distribution of SAR image amplitude.

It is known that the derivation of the Kalman filter is based on the assumption of an independent white Gaussian noise. From the previous section, the real amplitude value of image is considered as the observation noise when estimating the intensity of the scalloping. However, the distribution of SAR image amplitude is subject to the Rayleigh distribution, and the correlation between pixels makes the distribution not independent anymore. Fortunately, experimental results show that although the statistical distribution of the image does not satisfy the independent requirement or Gaussian distribution, the Kalman filter can still achieve accurate results, as long as the statistical distribution of each column does not deviate far from the Gaussian distribution.

To measure the difference between the statistical distribution of each column (corresponds to each frame in azimuth) and the Gaussian distribution, the Jarque-Bera test is introduced, to verify whether the data has the skewness and kurtosis that match the Gaussian distribution or not. The larger the J-B test result is, the more deviation from the Gaussian distribution. The Jarque-Bera test result can be calculated as follows [15].

$$J\text{-}B = \left[\frac{S^2}{6} + \frac{(K-3)^2}{24}\right] \tag{14}$$

where n is the number of observations, S is the skewness, and K is the kurtosis:

$$S = \frac{\frac{1}{n}\sum_{i=1}^{n}(x_i - \bar{x})^3}{\left[\frac{1}{n}\sum_{i=1}^{n}(x_i - \bar{x})^2\right]^{3/2}} \tag{15}$$

$$K = \frac{\frac{1}{n}\sum_{i=1}^{n}(x_i - \bar{x})^4}{\left[\frac{1}{n}\sum_{i=1}^{n}(x_i - \bar{x})^2\right]^{2}} \tag{16}$$

with $\bar{x}$ being the mean value of the data.

Simulation experiment is carried out to verify the influence of J-B values on the accuracy of scalloping estimation, using a GF-3 stripmap image without scalloping. And, the flowchart of the simulation is shown in Fig. 4. Firstly, each column of image is superimposed with a certain intensity of scalloping. And, to ensure that the simulated scalloping is appropriate, mean value of every column is used as the simulated scalloping intensity in this experiment. Then, the J-B value of each column calculated SAR image. Furthermore, Kalman filtering is performed on SAR image, and the relative estimating error of each column is calculated, as shown in Fig. 5.

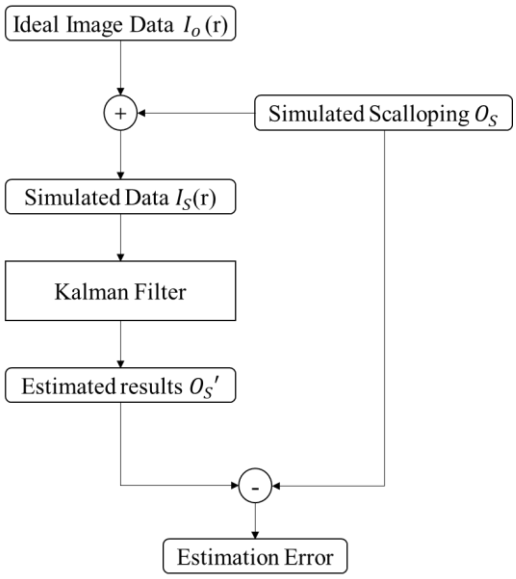

Fig. 4. Flowchart of simulation.

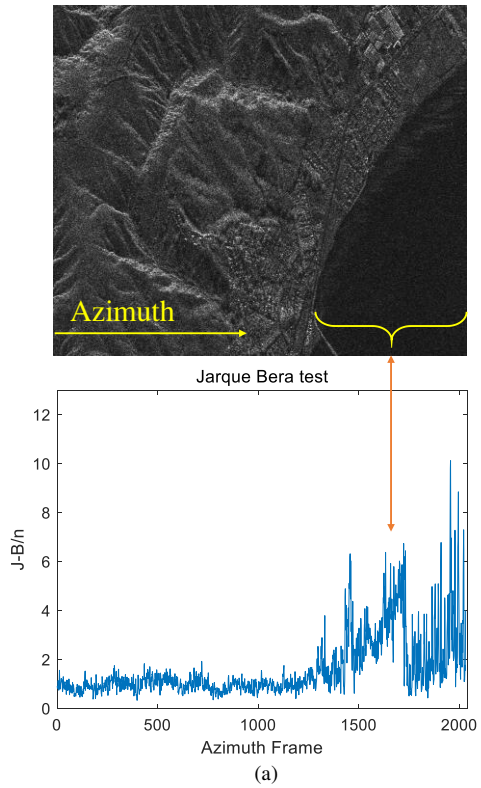

(a)

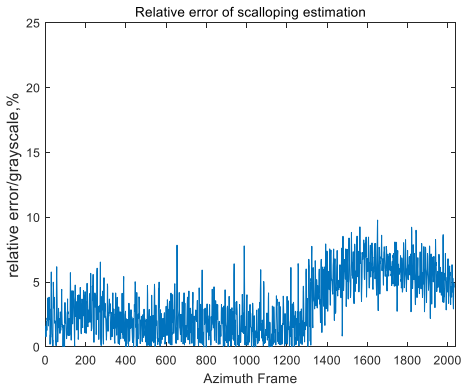

(b)

Fig. 5. (a) J-B valuse of image data for each azimuth frame; (b) relative error of the scalloping estimation reslut.

As shown in Fig. 5(a), it can be found that when the scene is stable, the J-B value is close to 0, which means the statistical distribution is close to the Gaussian distribution, and correspondingly, the relative estimation error is small (less than 5%) in Fig. 5(b). For sea-land boundary in image (around the 1400-2000 azimuth frame), there is a large difference in brightness between sea and land. Under these circumstances, the J-B values increase obviously, which means that the statistical distribution deviates from the Gaussian distribution and the relative estimation error increases significantly, as shown in Fig. 5(b). Therefore, it is particularly important to calculate J-B values, which is determined the performance of Kalman filtering results. If J-B values of the image are large, the Kalman filter becomes no longer applicable, and pre-processing becomes necessary, especially in the case of a complex scene.

IV. Proposed De-scalloping Method

In this section, a detailed method for scalloping removal in ScanSAR images is proposed. Firstly, the Jarque-Bera test is used to confirm whether the amplitude distribution of image satisfies the application requirements of the Kalman filter. If the image satisfies the requirements, the scalloping intensity estimation will be directly performed to obtain the final result. Otherwise, it is necessary to perform pre-processing, in which two sub-images that meet the Kalman filter's application condition will be produced. Then, scalloping intensity will be estimated in these two sub-images, respectively. Finally, the scalloping suppressed sub-images will be combined to reconstruct the final output image. The complete flow chart of the de-scalloping framework is shown in Fig. 6.

A. *Jarque-Bera Test*

The Jarque-Bera test is used in this method to evaluate whether the input image meets the application requirement of the Kalman filter. For the convenience of calculation, the J-B index of the entire image is directly calculated here to determine whether the input image needs to be pre-processed. Based on extensive experimental results, J-B=2.5 is chosen as the threshold.

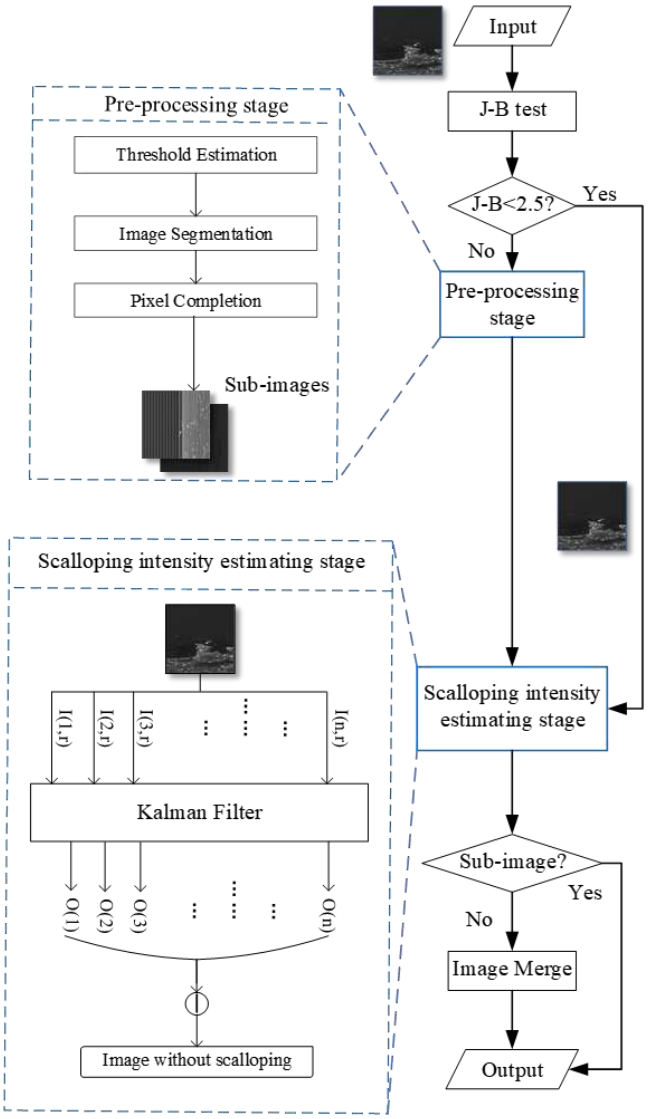

Fig. 6. Proposed de-scalloping procedure.

B. Pre-processing Method

The main purpose of the pre-processing method is to solve the problem that Kalman filter is not applicable when the distribution of image seriously deviates from the Gaussian distribution. The solution in this paper is to divide the image into two sub-images with different grayscale levels. Then, according to the statistical characteristics of data in each azimuth frame (column), the resulting missing pixels in the sub-images will be replaced. Through these two steps, the statistical distribution of data in column becomes closer to the Gaussian distribution, which ensures the scalloping suppression performance.

As for image division, the most important part is to estimate the appropriate threshold. In this paper, the maximum between-cluster variance (OTSU [16]) principle is used when choosing the threshold to ensure the maximum grayscale difference between sub-images. To save time for threshold calculation, a genetic algorithm is used for optimal threshold estimation. The fitness of the population is assessed using the between-class variance, which can be calculated by [17], [18]

$$\sigma_B = W_1 \cdot W_2 \left(\mu_1 - \mu_2\right)^2 \tag{17}$$

where W is the ratio of pixels in sub-image to all pixels and μ is the mean of the pixels in the sub-image. Then, the selection of the population uses the OTSU principle, whose aim is to find the threshold value with the maximum between-class variance.

Then, based on the threshold, the input image is divided into two sub-images, and the resulting missing pixels of each sub-image are needed to be replaced. On the one hand, the main purpose of pixel replacement is to make the data meet the application condition of Kalman filter. On the other hand, it must also be ensured that artificially generated pixels do not introduce new errors into the Kalman filter estimation. Therefore, this paper considers generating Gaussian random numbers to fill the missing pixels, based on the statistical properties of the original image. First, the mean and variance of the pixels are calculated according to the original image with each azimuth frame data. Next, Gaussian random numbers with the same mean and variance will be generated to fill the missing pixels in sub-images. It should be noted that if the proportion of pixels from the original image in an arbitrary column is extremely small, which means the mean and variance are not statistically significant, then the statistical properties of the nearby regions will be used. Consequently, after filling the missing pixels, two sub-images are suitable for Kalman filtering. Finally, all the artificially generated pixels will be eliminated when reconstructing the final output image.

C. Scalloping Intensity Estimation

This part uses the Kalman filter to estimate the intensity of scalloping, as shown in Fig. 6. A SAR image, with the size of $n \times m$ (Azimuth × Range), is divided into n sets of data: $I(1,r), I(2,r) \cdots\cdots I(n,r)$. Then, the Kalman filter is used to estimate the intensity of scalloping in each set of data to obtain $O(1), O(2) \cdots\cdots O(n)$. Subtracting $O(1), O(2) \cdots\cdots O(n)$ from the original image gives the final suppression result.

As for complex scenes (J-B>2.5), the sub-images are firstly processed with the same processing steps as described above. Then, for merging sub-images, the retained unfilled sub-images are used to determine whether the pixels in the sub-images are from the original input image or artificially generated. Only pixels from the original image will be preserved, so a complete output image is obtained with scalloping suppression.

V. Experiments

Experiments are carried out to demonstrate the effectiveness of the proposed method, using ScanSAR images of simulated data, GF-3 and TerraSAR-X, respectively. The simulated images are used to verify that the pre-processing method can modify the statistical distribution of data, and thus reduce the estimation error of Kalman filter for scalloping estimation. Then, the de-scalloping results using real ScanSAR images (GF-3 and TerraSAR-X) are provided with detailed analysis.

A. *Verification of the Pre-processing Method*

In order to verify the effectiveness of the pre-processing method, a GF-3 stripmap image (as shown in Fig. 5) is used. The image segmentation threshold is estimated by a genetic algorithm. The image segmentation result is shown in Fig. 7(a), and the missing pixels on the sub-image 1 and sub-image 2 are filled, as shown in Fig. 7 (b).

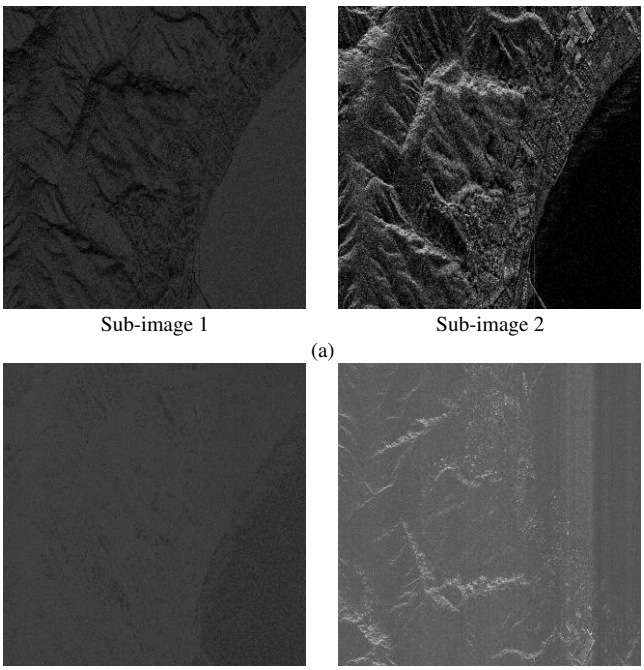

Fig. 7. (a) Image segmentation result. (b) Sub-image after pixel filling.

Then, the J-B values and scalloping estimation error of data in each azimuth are calculated. The results are shown in Fig. 8 and Fig. 9.

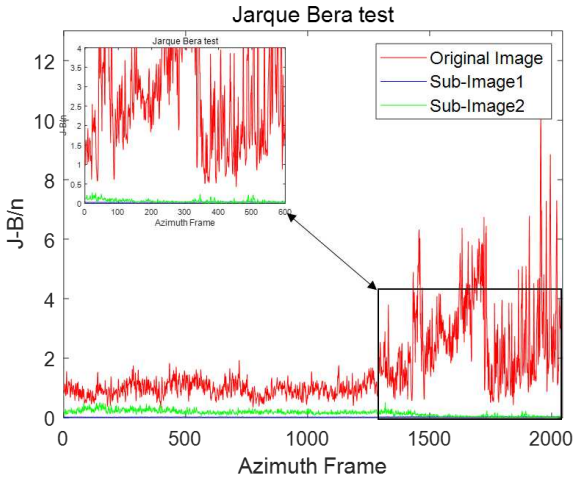

Fig. 8. Jarque-Bera test results of original image (red line) and two sub-images (blue line and green line).

As shown in Fig. 8, after pixel filling, the J-B values of sub-image 1 and sub-image 2 become stable and below the threshold (J-B<2.5), which means that the pixel filling method works well.

Furthermore, simulation experiments similar to Section III are carried out. Each azimuth frame is superimposed the same scalloping, as Fig. 5(a). Then, performing the proposed scalloping suppression on sub-images, the relative estimation errors are shown in Fig. 9.

As shown in Fig. 9, it can be found that the relative scalloping estimation error of sub-images is below 5%. Comparing with Fig. 5(b), the relative error has increased significantly in the sea-land area (around the 1400-2000 azimuth frame). The results indicate that the pre-processing scheme is able to control the relative scalloping estimation error effectively, especially in the case of a complex scene.

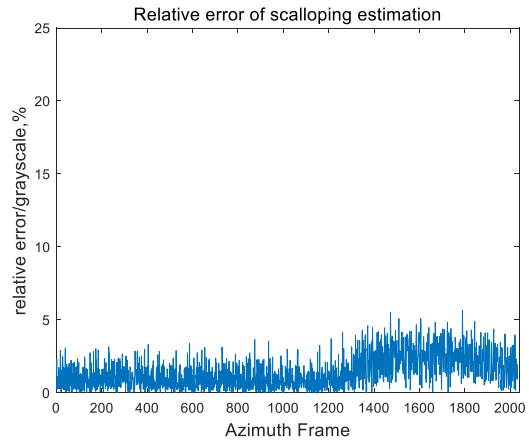

(a) Relative estimation error of each azimuth frame in sub-image 1.

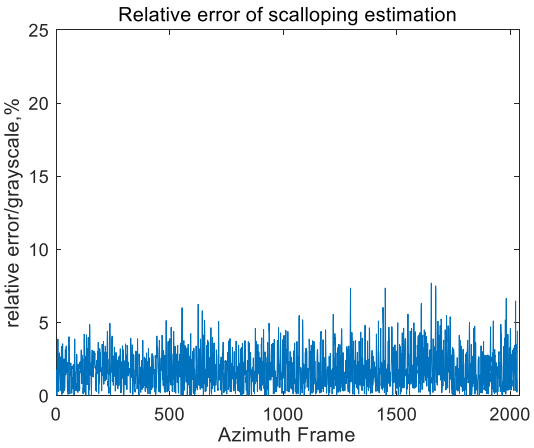

(b) Relative estimation error of each azimuth frame in sub-image 2.

Fig. 9. Relative error of scalloping intensity estimation.

B. *Scalloping Suppression Results*

1) *Stationary scene (J-B<2.5) processing result*

Data used in this part comes from the GF-3 satellite, working in the narrow scan mode. In this part, some stationary scene images are selected and they do not need to be pre-processed. The Kalman filter can be used to estimate scalloping intensity directly. Fig. 10 shows the experimental results.

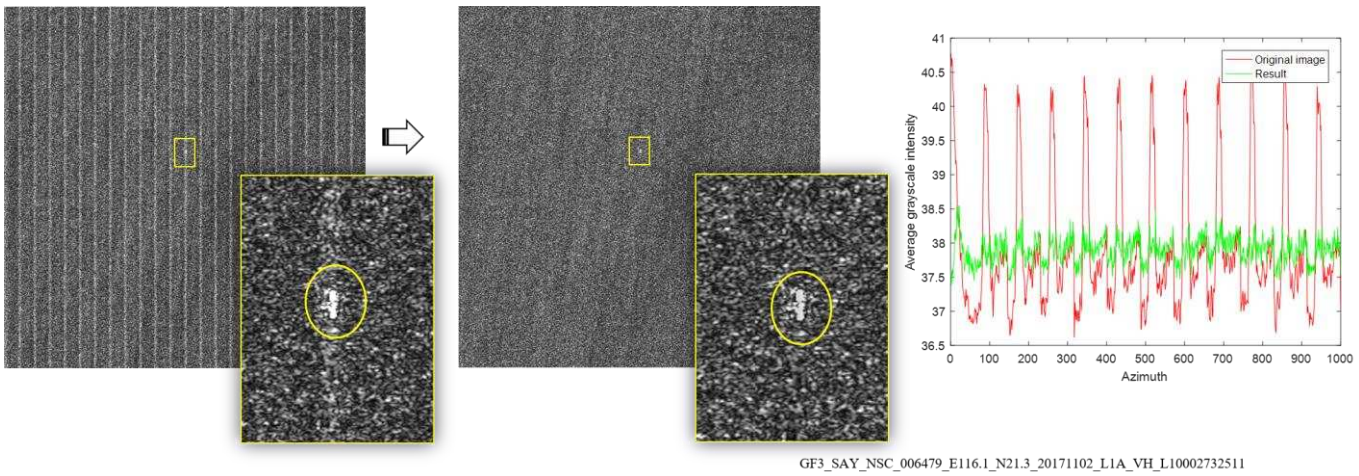

(a)

(b)

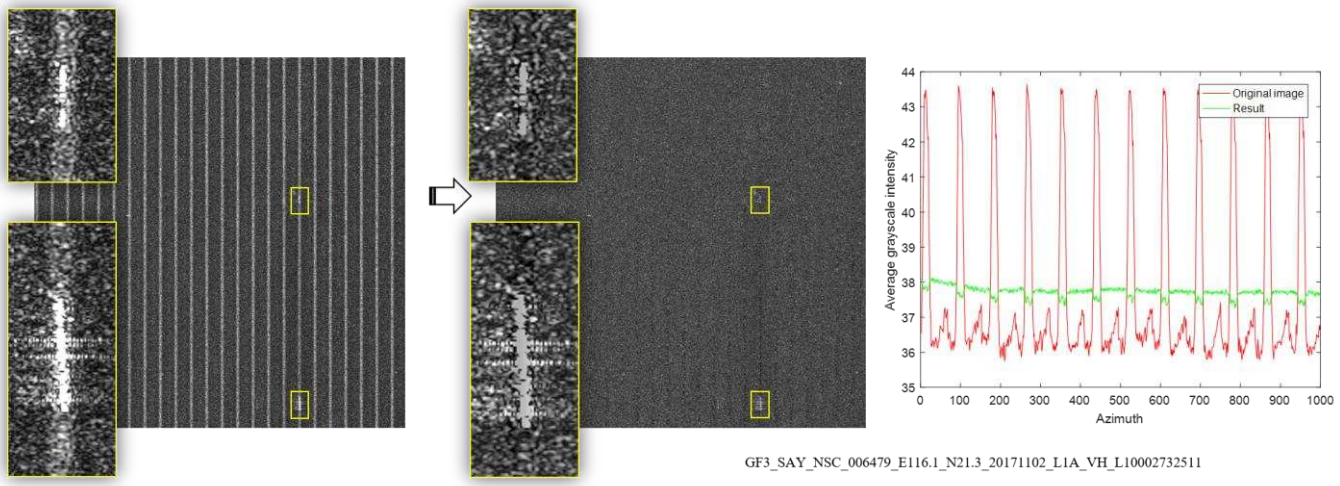

(c)

Fig. 10. Processing results for three sets of stationary scenes (J-B<2.5). Left: original image. Middle: scalloping suppression result. Right: the average grayscale intensity profile.

Fig. 10 (a) shows the image processing result with an ocean scene. Comparing the images before and after processing, it can be seen that scalloping is significantly suppressed. The graph on the right shows the average grayscale intensity of each azimuth frame in the original image and the resultant image. The curve reflects the fluctuation of data energy in each azimuth frame. The average grayscale intensity (AGI) of a column is calculated as follows [10].

$$AGI(a)=20\cdot\log\left[\frac{\sum_{i=1}^{r} I(a,i)}{r}\right] \tag{18}$$

The figure shows the average grayscale intensity profiles of the original image and the resultant image respectively (around 1000 range bins are selected). The curve of the original image (red line) exhibits severe fluctuations due to the scalloping effect. After processing, the abnormal fluctuation has been suppressed greatly in the profile of the resultant image (green line).

In addition, it is necessary to pay attention to whether the scalloping suppression affects the targets in the image. An enlarged view of a target is shown in Fig. 10 (a). It can be seen that the target is still clearly visible after scalloping suppression. This will be discussed further in the following section.

Fig. 10 (b) is the processing result of a land scene image. It can be seen that the scalloping effect in the original image has been effectively suppressed. The average grayscale intensity profiles also lead to the same conclusion. Furthermore, for the part that contains the river (enlarged part), in the original image, the river is covered by scalloping, and it is difficult to distinguish it from the background; after processing, the originally covered texture is revealed.

Fig. 10 (c) shows the results of another ocean scene with ship targets, and the scalloping effect in this image is more severe than that in Fig. 10 (a). It can be seen from the result that the proposed method can still achieve satisfactory results in such a serious scalloping situation. The profiles of the average grayscale intensity also show that the scalloping effect has been suppressed effectively. The special feature of this image is that two targets are almost overlapped with scalloping as shown in the enlarged figures. It can be seen intuitively from Fig. 10 (c) that after processing, although the target can still be distinguished, the energy of the target is lost. The reason may be that the target and the scalloping are almost in parallel, causing estimation error of the Kalman filter. Nevertheless, this problem does not really affect the effectiveness of this method: on the one hand, it is a very low probability event that the target is in parallel to the scalloping pattern and completely covered. on the other hand, even if this kind of situation occurs, the target is still detectable.

2) Processing Result for Non-stationary Scene (J-B>2.5)

The so-called non-stationary scene refers to images of complicated scenes, which means part of image data does not meet the application condition of the Kalman filter. Based on extensive experimental results, the threshold value 2.5 (J-B parameter) is chosen to determine whether pre-processing is necessary or not. When the J-B parameter of the image is larger than 2.5, the image is considered to be non-stationary, and the pre-processing is required. This subsection shows the processing results of four non-stationary images and we compare them with the results using the method in [11].

Fig. 11 displays the results of an image containing both ocean and land. In the sea-land junction area, the method in [11] has a poor performance for scalloping suppression, even resulting in more serious scalloping than the original image. As for the proposed method, it works well in the whole image, especially in the sea-land junction area. And, the average grayscale intensity profile is shown also in the figure. The blue line reflects the fluctuations in the results obtained by the method of [11], from which it can be seen that the fluctuation is more severe than the original image in the sea-land junction area. The green line reflects the fluctuations of the results using the proposed method, which is less than the original and therefore smoother.

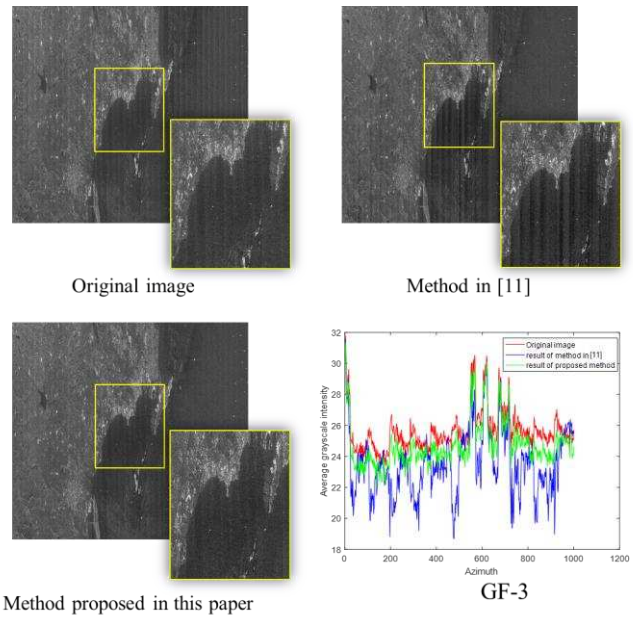

Fig. 11. Original image and results processed by the two methods and the average grayscale curve (Red line: the original image; Blue line: result processed by the method in [11]; Green line: result obtained by the proposed method).

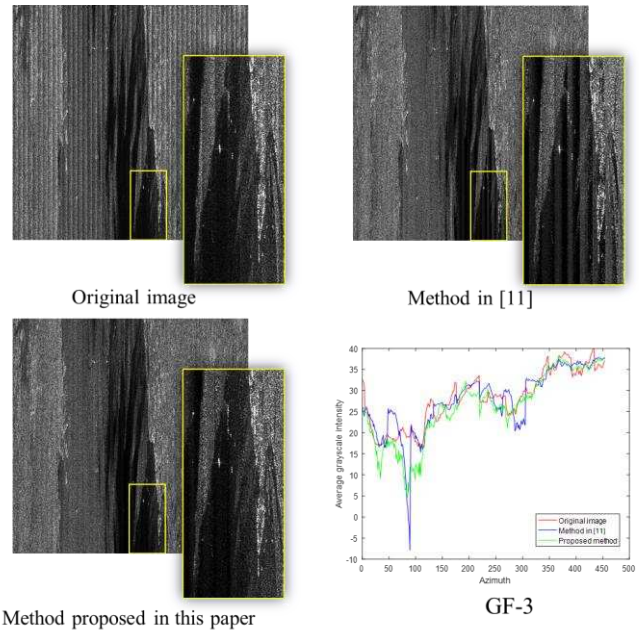

Fig. 12. Original image and results processed by the two methods and the average grayscale curve (Red line: the original image; Blue line: result processed by the method in [11]; Green line: result obtained by the proposed method).

Fig. 12 shows another set of experimental results. The special feature of the original image is that the scalloping is not constant (there is almost no scalloping in the dark area of the image). After being processed by the method in [11], most of the scalloping in the image is effectively suppressed, but unexpected bright stripes appear in the dark area. Using the proposed method, the scalloping is also effectively suppressed, and there is no artificial artifact in this area. It can be seen from the profile that there is abnormal fluctuation in the blue line (the method in [11]). In contrast, the curve obtained by the method in this paper (green line) is less volatile than the original one.

Fig. 13 is a ScanSAR image from TerraSAR-X. It also includes areas of sea-land junctions. The proposed method suppresses the scalloping more effectively than the method in [11]. It can be seen from the enlarged part, especially in the ocean part, that the processing performance of the proposed method is obviously better. Moreover, according to the average grayscale profiles, the fluctuation in the green line has been significantly suppressed, while the blue line still fluctuates intensely. It is worth mentioning that after the scalloping suppression, the detail of the mountains in the resultant image is clearer than before.

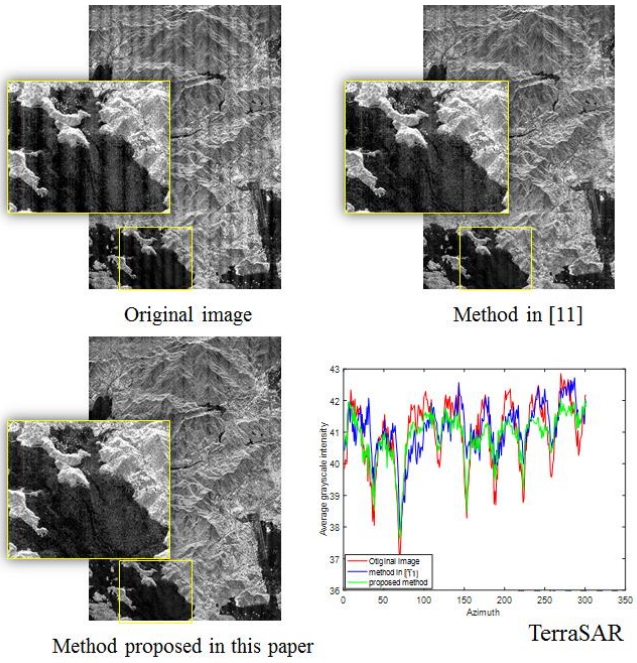

Fig. 13. Original image and results processed by the two methods and the average grayscale curve (Red line: the original image; Blue line: result processed by the method in [11]; Green line: result obtained by the proposed method).

Fig. 14 presents the experimental results of a GF-3 ScanSAR image containing the sea-land junction scene. Scalloping in this image is more severe than that in the previous three images. After processing, the results of both methods show that the scalloping is significantly suppressed. However, the scalloping in the sea-land junction part is not effectively suppressed using the method [11]. Similar to Fig. 11, artificial artifact appears in image. After calculating the average grayscale profiles of the enlarged area, it can be seen from the results that the method proposed is obviously better for dealing with the sea-land junction scene.

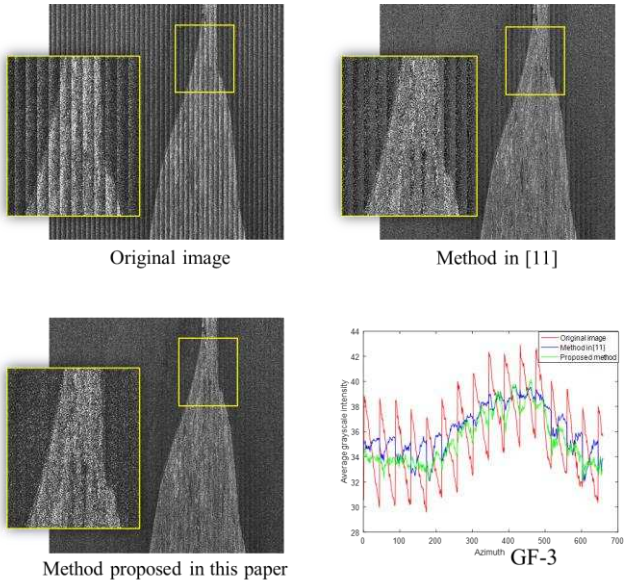

Fig. 14. Original image and results processed by the two methods and the average grayscale curve (Red line: the original image. Blue line: result processed by the method in [11]. Green line: result obtained by the proposed method.).

In addition, observing the images before and after processing, it can be found that the edge of the land in the original image is blurred, while the edge becomes clearer after scalloping suppression. In order to verify the above observation, edge detection is performed in Fig. 15 using the edge function in MATLAB, choosing the ‘roberts’ operator.

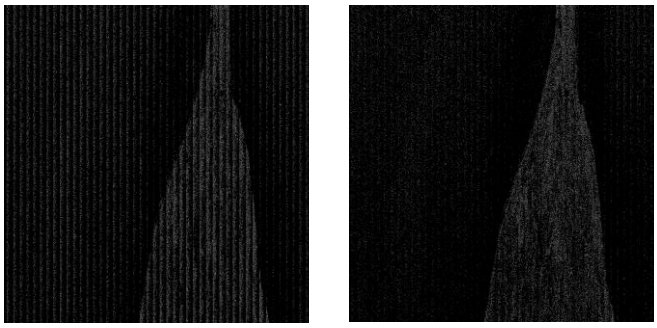

(a) (b)

Fig. 15. Edge detection result: (a) original image; (b) result.

In Fig. 15 (a), the stripes of scalloping are detected and the edge of the land is blurred by the scalloping. After scalloping suppression, the stripes disappear and the edge becomes clearer.

In summary, the proposed method can achieve satisfactory processing results with robustness in response to complicated situations.

C. Further Discussion

Firstly, in order to verify the ability of target preservation, two targets are selected for analysis.

As shown in Fig. 16, scalloping is not serious and the targets are not covered by scalloping. After processing, there is almost no loss of target energy. However, when the scalloping is very serious and completely covers the target, it may cause the following problems: On the one hand, target brightness is very strong, which may affect the scalloping intensity estimation; on the other hand, the scalloping suppression may also cause target energy loss. In order to verify the effectiveness of the method in this situation, two targets covered by scalloping stripes are selected for analysis. Fig. 17 shows the energy of the targets before and after processing. In these two sets of experimental results, the scalloping is effectively suppressed. The target energy is only slightly reduced, which hardly affects the subsequent application of the images.

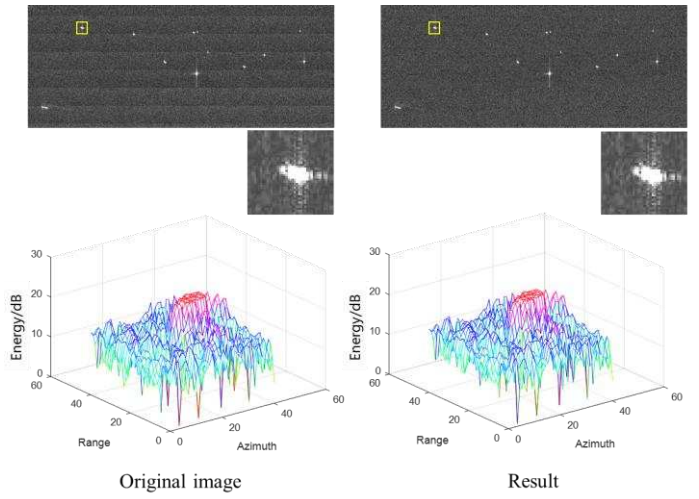

(a)

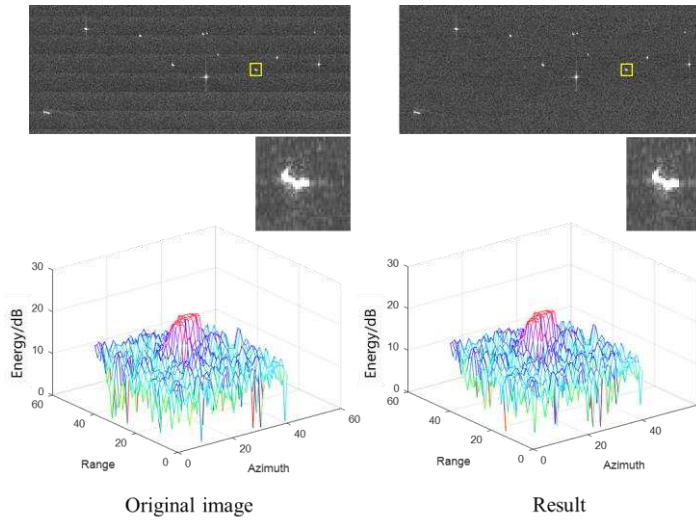

(b)

Fig. 16. Point target energy map, where the left side is the results of the original image and the right side the results after processing.

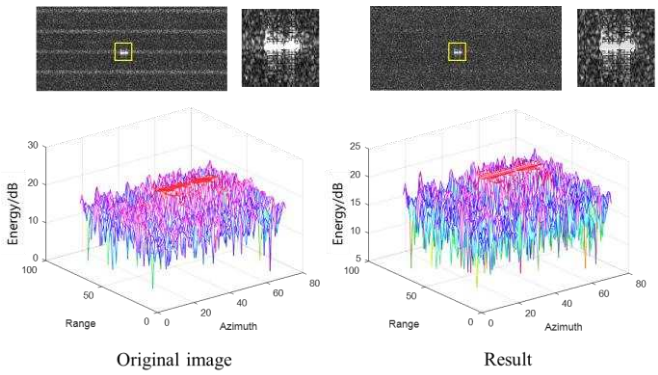

(a) Scalloping covered target1

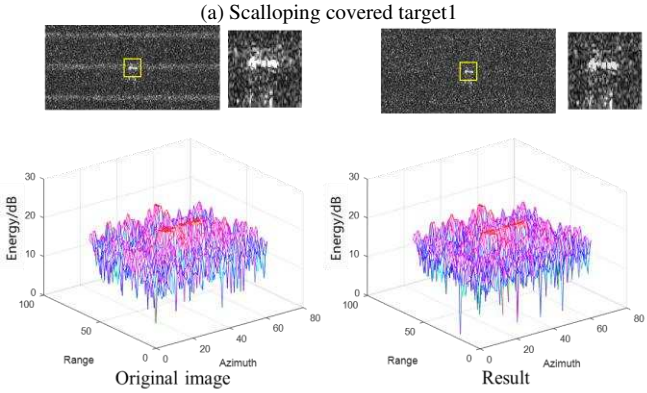

(b) Scalloping covered target2

Fig.17. Target energy map, where the left side is the results of the original image and the right side is the results after processing.

To further verify the effectiveness of the proposed method, a GF-3 image is selected, illuminating the urban area of ShangHai, China. As shown in Fig. 18, the scalloping is suppressed significantly, which proves that the proposed method can deal with the image with building intensive area.

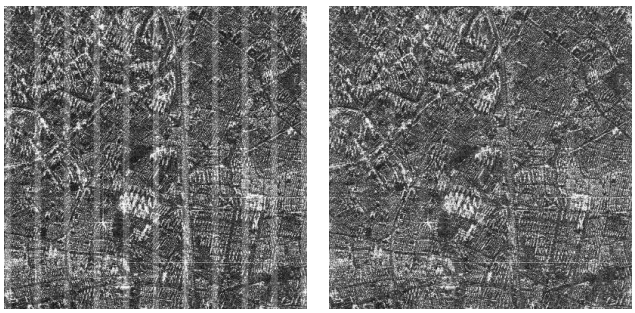

(a) Before scalloping suppression (b) After scalloping suppression

Fig. 18. Scalloping suppression results of urban area

The mean value, variance and residual scalloping effect in the images after processing are also calculated. The results are shown in Table. I. The variance is reduced after processing, which can be considered as a result of the scalloping being suppressed. And, the intensity of the scalloping in the results is greatly reduced (1.52dB-8.84dB), which means that the proposed method can effectively suppress the scalloping. As for the mean value of the images, it does not change much after processing. Note that the power of the scalloping effect is strong in Fig. 14, therefore the mean of original image is a little larger than the processing results, due to the removal of scalloping energy.

As a summary, by adding the pre-processing operation before Kalman filtering, the proposed method can accommodate different complex scene and achieve good performance for scalloping suppression, which is verified by GaoFen-3 (GF-3) and TerraSAR-X satellite images.

TABLE I
INDICATORS OF THE IMAGES USED IN THIS PAPER

		Mean	Variance	Scalloping
Fig. 10(a)	Original	77.65	1.79e+3	2.87dB
	Result	76.84	1.69e+3	0.51dB
Fig. 10(b)	Original	78.53	2.11e+3	6.49dB
	Result	75.71	1.39e+3	0.38dB
Fig. 10(c)	Original	42.81	838.17	4.98dB
	Result	43.37	755.29	0.26dB
Fig. 11	Original	30.33	605.11	1.73dB
	Result	29.71	599.88	0.17dB
Fig. 12	Original	63.45	2.17e+3	5.57dB
	Result	60.37	2.02e+3	0.69dB
Fig. 13	Original	114.22	3.42e+3	2.41dB
	Result	113.72	3.24e+3	0.89dB
Fig. 14	Original	63.98	1.93e+3	9.08dB
	Result	57.18	1.38e+3	0.24dB

VI. CONCLUSION

The scalloping suppression problem in ScanSAR images has been studied in this work by employing the Kalman filtering for scalloping intensity estimation. In order to solve the problem that the Kalman filter fails in some complex scenes, the application conditions of Kalman filter are analyzed by the Jarque-Bera test. On this basis, a pre-processing method for complex scenes is proposed, including image segmentation and pixel value filling. Moreover, a complete scalloping suppression method that can handle various situations is proposed. Simulation results show that the pre-processing method can effectively reduce the relative error of scalloping intensity estimation. Finally, the performance is verified by GaoFen-3and TerraSAR-X satellite images with different scenes. The results demonstrate that the proposed method can accommodate the complex scene well and achieve effective scalloping suppression.

REFERENCES

[1] H. Wang and X. Jia, "Improvement of image resolution in ScanSAR simulation", in *3rd CISP*, Yantai, China, Oct. 2010.

[2] S. Wollatadt *et al.,* "Scalloping correction in TOPS imaging mode SAR data", *IEEE Geosci. Remote Sens. Lett.*, vol. 9, no. 4, pp. 614-618, Jul. 2012.

[3] M. Shimada. "A new method for correcting ScanSAR scalloping using forests and inter-Scan banding employing dynamic filtering", *IEEE Trans. Geosci. Remote Sens.*, vol. 47, no. 12, pp. 3933 – 3942, Sep. 2009.

[4] N. Li, et al., "Processing sliding mosaic mode data with modified full-aperture imaging algorithm integrating scalloping correction", *IEEE J-STARS*, Vol. 10, no. 5, pp. 1804-181, May. 2017.

[5] R. Bamler, "Optimum look weighting for burst-mode and ScanSAR processing", *IEEE Trans. Geosci. Remote Sens.,* vol.33, no. 3, pp. 722-725, May. 1995.

[6] M. Shimada, "Long-term stability of L-band normalized radar cross section of Amazon rainforest using the JERS-1 SAR", *Canadian J. of Remote Sensing*, vol. 31, no. 1, pp. 132-137, 2005.

[7] M. Shimada *et al.*, "PALSAR radiometric and geometric calibration", *IEEE Trans. Geosci. Remote Sens.,* vol. 4, no. 13, pp. 3915-3932, Dec. 2009.

[8] U. Balss, H. Breit, T. Fritz, "Noise-related radiometric correction in the TerraSAR-X multimode SAR processor", *IEEE Trans. Geosci. Remote Sens.*, vol.48, no. 2, Feb. 2010.

[9] R. Romeiser *et al*., "A new scalloping filter algorithm for scansar images" in *IGARSS*, Honolulu, HI, USA. pp. 4079-4082, Jul. 2010.

[10] A. Sorrentino *et al*., "A post-processing technique for scalloping suppression over ScanSAR images", in *EUCAP*, Prague, Czech Republic. pp. 2164-3342, Jun. 2012.

[11] M. Iqbal *et al.*, "Kalman filter for removal of scalloping and inter-scan banding in scansar images", *Progress in Electromagnetics Research*, vol. 132, no. 5, pp. 443-461, Sep. 2012.

[12] G. Xinwei *et al.*, "Suppression of scalloping and inter-Scan banding in non-stationary ScanSAR images based on Kalman filter and image segmentation", *Journal of Naval Aeronautical and Astronautical University,* vol. 132, no.5, pp. 125-129+134, Dec. 2017.

[13] A. M. Guarnieri, C. Prati, "ScanSAR focusing and interferometry", *IEEE Trans. Geosci. Remote Sens.,* vol.34, no. 4, pp. 1029-1038, Jul. 1996.

[14] R. Dieversi *et al.*, "Kalman filtering in extended noise environments", *IEEE Trans. Automat. Contr.* vol. 50, no. 9, pp. 1396-1402, Sep. 2005.

[15] D. Bradley *et al.*, "On the performance of negentropy approximations as test statistics for detecting sinusoidal RFI in microwave radiometers", *IEEE Trans. Geosci. Remote Sens.,* vol.51, no. 10, pp. 4945-4951, Oct. 2013.

[16] N. Otsu, "A threshold selection method from gray-level histograms," *IEEE Transactions on Systems, Man, and Cybernetics*, vol. 9, no. 1, pp. 62–66, Jan 1979.

[17] Q. Chen *et al.*, "Modified two-dimensional otsu image segmentation algorithm and fast realisation" *IET Image Processing,* vol. 6, no. 4, pp. 426-433, Jun. 2012.

[18] H. Ye, S. Yan, P. L. Huang, "2D Otsu image segmentation based on cellular genetic algorithm", in *ICCSN*, Guangzhou, China, pp. May 2017.